Title	Determining the ^{239}Np(n,f) cross section using the surrogate ratio method
Author(s)	Czeszumska A., Angell C., Burke J. T., Scielzo N. D., Norman E. B., Austin R. A. E., Boutoux G., Casperson R. J., Chodash P., Hughes R. O., Mattoon C. M., Méot V., Munson J., Phair L., Ressler J. J., Roig O., Ross T. J., Swanberg E., Wang B.
Citation	Physical Review C, 87(3), p.034613_1-034613_6
Text Version	Publisher's Version
URL	https://jopss.jaea.go.jp/search/servlet/search?5040005
DOI	https://doi.org/10.1103/PhysRevC.87.034613
Right	

Determining the ^{239}Np(n, f) cross section using the surrogate ratio method

A. Czeszumska,[1,*] C. T. Angell,[1,2] J. T. Burke,[3] N. D. Scielzo,[3] E. B. Norman,[1,3,4] R. A. E. Austin,[5] G. Boutoux,[6,7] R. J. Casperson,[3] P. Chodash,[1] R. O. Hughes,[8] C. M. Mattoon,[3] V. Méot,[9] J. Munson,[1] L. Phair,[4] J. J. Ressler,[3] O. Roig,[9] T. J. Ross,[8,10] E. Swanberg,[1] and B. Wang[1]

[1]*Department of Nuclear Engineering, University of California, Berkeley, California 94720, USA*
[2]*Quantum Beam Science Directorate, Japan Atomic Energy Agency, Tokai-mura, Ibaraki 319-1195, Japan*
[3]*Physics Division, Lawrence Livermore National Laboratory, Livermore, California 94550, USA*
[4]*Nuclear Science Division, Lawrence Berkeley National Laboratory, Berkeley, California 94720, USA*
[5]*Saint Mary's University, Halifax, Canada*
[6]*CNRS, IN2P3, CENBG, UMR 5797, F-33175 Gradignan, France*
[7]*Université de Bordeaux, CENBG, UMR 5797, F-33175 Gradignan, France*
[8]*Department of Physics, University of Richmond, Richmond, Virginia 23173, USA*
[9]*CEA DAM DIF, F-91297 Arpajon, France*
[10]*Department of Physics, University of Surrey, Guildford GU2 7XH, United Kingdom*

(Received 23 December 2012; published 12 March 2013)

Background: Neutron-induced fission cross-section data are needed in various fields of applied and basic nuclear science. However, cross sections of short-lived nuclei are difficult to measure directly due to experimental constraints.

Purpose: The first experimental determination of the neutron-induced fission cross section of ^{239}Np at nonthermal energies was performed. This minor actinide is the waiting point to ^{240}Pu production in a nuclear reactor.

Method: The surrogate ratio method was employed to indirectly deduce the ^{239}Np(n, f) cross section. The surrogate reactions used were ^{236}U(^{3}He, p) and ^{238}U(^{3}He, p) with the reference cross section given by the well-known ^{237}Np(n, f) cross section. The ratio of observed fission reactions resulting from the two formed compound nuclei, ^{238}Np and ^{240}Np, was multiplied by the directly measured ^{237}Np(n, f) cross section to determine the ^{239}Np(n, f) cross section.

Results: The ^{239}Np(n, f) cross section was determined with an uncertainty ranging between 4% and 30% over the energy range of 0.5–20 MeV. The resulting cross section agrees closest with the JENDL-4.0 evaluation.

Conclusions: The measured cross section falls in between the existing evaluations, but it does not match any evaluation exactly (with JENDL-4.0 being the closest match); hence reactor codes relying on existing evaluations may under- or overestimate the amount of ^{240}Pu produced during fuel burnup. The measurement helps constrain nuclear structure parameters used in the evaluations.

DOI: 10.1103/PhysRevC.87.034613 PACS number(s): 24.87.+y, 25.85.Ge, 25.85.Ec, 25.55.−e

I. INTRODUCTION

The recent interest in new Generation-IV nuclear reactor designs, many of which utilize fast neutrons [1], has increased the need for accurate data for neutron-induced reactions. Cross-section data, even of minor actinides, may alter reactor neutronics and burnup and are needed to engineer safer and more proliferation-resistant reactors. In addition, accurate neutron-induced reaction cross sections are needed for understanding nucleosynthesis, as well as for stockpile stewardship and nuclear waste management applications.

The ^{239}Np(n, f) cross section plays a role in the proliferation-resistance aspect of a reactor design, as ^{239}Np is on a waiting point to ^{239}Pu and ^{240}Pu production (see Fig. 1). As neutron-induced fission on ^{239}Np removes actinide nuclei from the chain, knowing its fission cross section in relation to its neutron capture cross section would help predict the amount of ^{239}Pu and ^{240}Pu produced in the reactor. A higher ^{240}Pu to ^{239}Pu production ratio may be desirable, as it renders the spent fuel less weapons-usable because of the difficulty of separating plutonium isotopes from one another.

Direct measurements of neutron-induced reaction cross sections of short-lived nuclei, such as ^{239}Np (whose half-life is 2.36 days), are impeded by the challenges of amassing the required target material and the background from the decaying nucleus. Hence, one has to resort to an indirect measurement technique, such as the surrogate ratio method (SRM). This approach was first used by Cramer and Britt [2] in 1970, and more recently it has been benchmarked and used to determine several cross sections [3–9].

This paper reports the experimental measurement of the ^{239}Np(n, f) cross section, performed using the SRM. The SRM is described in Sec. II. Section III details the experimental setup. Section IV guides the reader through analysis steps, shows final results, and discusses uncertainties. In Sec. V, discussion of the results compares the measurement to existing evaluations. Lastly, Sec. VI concludes the paper with some final remarks and possibilities for the future.

*agac@berkeley.edu

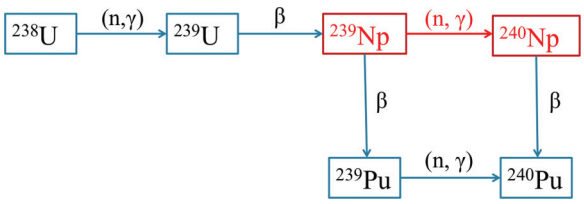

FIG. 1. (Color online) Production chain of ^{239}Np, ^{239}Pu, and ^{240}Pu.

II. SURROGATE RATIO METHOD

In the surrogate method, a direct reaction is used to form the same compound nucleus (CN) that would be formed in the difficult-to-measure desired reaction. Using a direct reaction allows one to choose an experimentally accessible ion beam and target combination. The central assumption behind the surrogate method is that the decay branching ratios of the compound nucleus are independent of the spin and parity of its populated states, and hence the CN decay is independent of its formation mechanism. Known as the Weisskopf-Ewing limit [10] under Hauser-Feshbach theory [11], the assumption is expected to hold above neutron energies of 1 MeV [12,13]. With this assumption, one can describe the cross section as follows [12]:

$$\sigma(n,\,f)(E) = \sigma_n^{\rm CN} P_{\delta f}^{\rm CN}(E), \tag{1}$$

where $\sigma_n^{\rm CN}$ is the formation cross section of the compound nucleus with the desired reaction, $P_{\delta f}^{\rm CN}(E)$ is the decay probability into the desired fission exit channel f of the compound nucleus formed via the direct reaction δ, and E is the excitation energy of the nucleus. While $\sigma_n^{\rm CN}$ can be calculated with an optical model, $P_{\delta f}^{\rm CN}(E)$ can be measured as follows:

$$P_{\delta f}^{\rm CN}(E) = \frac{N_{\delta f}(E)}{\epsilon_f N_\delta(E)}, \tag{2}$$

where $N_{\delta f}(E)$ is the total number of measured particle-fission coincident events (where the particle identifies the compound nucleus formed), ϵ_f is the fission detector efficiency, and $N_\delta(E)$ is the total number of direct reactions that formed the compound nucleus. The last term can be expressed as

$$N_\delta(E) = \rho Q \epsilon_\delta l \sigma_\delta(E), \tag{3}$$

where ρ is the areal density of the target, Q is the total number of projectiles delivered to the target, ϵ_δ is the efficiency for detecting the direct reaction, l is the detector live time fraction, and $\sigma_\delta(E)$ is the direct reaction cross section. However, due to backgrounds from contaminants in the target and the target backing, the total number of reactions is difficult to determine reliably. This problem can be avoided by using a ratio of two reactions on similar target nuclei (the SRM) [4,6]. Combining Eqs. (1), (2), and (3) yields the ratio

$$\frac{\sigma_1(n,\,f)(E)}{\sigma_2(n,\,f)(E)} = \frac{\sigma_{n1}^{\rm CN}(E) N_{\delta 1 f}(E) \epsilon_{f2} \epsilon_{\delta 2} \sigma_{\delta 2}(E)}{\sigma_{n2}^{\rm CN}(E) N_{\delta 2 f}(E) \epsilon_{f1} \epsilon_{\delta 1} \sigma_{\delta 1}(E)} \times C, \tag{4}$$

where C is a constant consisting of experimentally measured terms [shown in Eq. (3)]:

$$C = \frac{\rho_{T_2} l_2 Q_2}{\rho_{T_1} l_1 Q_1}. \tag{5}$$

For target nuclei that are similar (nearby in atomic number, with similar ground-state spins), the formation cross sections for both reactions are expected to be similar, i.e., $\frac{\sigma_{\delta 2}(E)}{\sigma_{\delta 1}(E)} \approx 1$ and $\frac{\sigma_{n1}^{\rm CN}(E)}{\sigma_{n2}^{\rm CN}(E)} \approx 1$ [5]. In addition, if the detector setup for both of the surrogate reactions is the same, the ratio of particle detector efficiencies is unity ($\frac{\epsilon_{\delta 2}}{\epsilon_{\delta 1}} \approx 1$) and the ratio of the fission detector efficiencies is also unity ($\frac{\epsilon_{f2}}{\epsilon_{f1}} \approx 1$), if the fission fragment angular distribution is similar for both targets, i.e. the fission anisotropy ratio approaches unity. Fission anisotropy is discussed in Sec. IV B.

If the second surrogate reaction in the ratio is used to determine a well-known cross section, it is possible to extract the unknown cross section. In this work, the measured ratio of the two surrogate reactions, ^{238}U(^{3}He, p)^{240}Np and ^{236}U(^{3}He, p)^{238}Np, was normalized to the known ^{237}Np(n, f) cross section [14], resulting in a determination of the unknown ^{239}Np(n, f) cross section. From Eq. (4), the final relation used for determining the cross section with the SRM was

$$\sigma_{(n,f)}^{^{239}Np}(E) = \sigma_{(n,f)}^{^{237}Np}(E) \frac{N_{(p,f)}^{^{240}Np}}{N_{(p,f)}^{^{238}Np}} C, \tag{6}$$

where $N_{(p,f)}^{^{240}Np}$ and $N_{(p,f)}^{^{238}Np}$ signify the number of experimentally measured compound nuclei formed through the surrogate reactions and resulting in fission events. In this case, the number of protons in coincidence with fission was measured to assess the number of fissioning compound nuclei formed via the (^{3}He, p) reaction.

III. EXPERIMENT

The experiment was performed over a three-day period at the 88-Inch Cyclotron at Lawrence Berkeley National Laboratory, using a 29-MeV ^{3}He beam on ^{236}U and ^{238}U targets. The two targets were exchanged about every hour throughout the experiment to account for possible changes in the beam intensity and the detector gains occurring over the period of the experiment. The ^{238}U and ^{236}U targets were irradiated for 21 and 23 h, respectively.

The experimental setup consisted of the standard Silicon Telescope Array for Reaction Studies (STARS) [15], with an additional array of six room-temperature lithium-drifted Ortec L-series silicon detectors. The setup schematic is shown in Fig. 2.

Two Micron Semiconductor S2 double-sided silicon detectors stacked together, referred to as the ΔE (140 μm) and E (1000 μm) detectors, were used to identify the light ions. An aluminum holder with an array of six circular L-series detectors, each 5000 μm thick with an active area of 200 mm^2 and pointing concentrically toward the target at 45°, was placed behind the E detector to stop protons up to 30 MeV in energy. A degrader foil of 4.44 mg/cm^2 Al, biased to 300 V, was used to stop δ electrons and fission fragments from reaching the ΔE detector. Upstream from the target, another 140-μm-thick S2 silicon detector was placed to detect fission fragments. The S2 detectors were instrumented into 8 sector channels and 24 ring channels for the electronics readout.

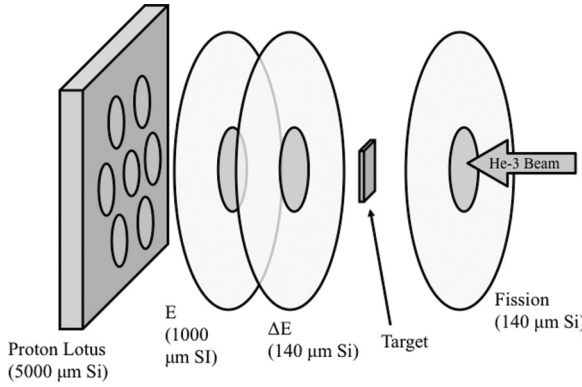

FIG. 2. Components of the experimental setup.

The particle telescope energy response was calibrated using a ^{226}Ra α source. Calibration of the fission detector with a ^{252}Cf source assessed the energy straggle of the fission fragments in the detector.

The target areal density was approximately 320 μg/cm^2 for ^{236}U and 220 μg/cm^2 for ^{238}U. Each target was electroplated onto a 100 μg/cm^2 natural carbon backing. The ratio of the target areal densities between the two targets, comprising the value used to normalize the ^{239}Np cross section data, was determined experimentally from the ratio of the recorded fusion-fission events of the two targets. The fission detector was used to record the number of events, and only events above approximately 25 MeV in energy were considered to ensure exclusion of light-ion events from the analysis. (The energy threshold is shown in Fig. 4.) The data were obtained from averaging the result of five different run pairs, each yielding a ratio of ^{238}U to ^{236}U fusion-fission events. Each pair was chosen so that their average beam current was similar to within 2%, in order to reduce any rate-dependent effects. Since this measured ratio of events depends on the fusion-fission cross section ratio between the two targets, the nuclear reaction modeling code EMPIRE [16] was used to model the total ^{3}He-induced fission cross section for each target and extract the cross-section ratio. Calculations were done with and without coupled channels to estimate the sensitivity of the ratio. The average value of the ^{238}U/^{236}U cross section ratio, across the ^{3}He energy range of 26–30 MeV, was found to be 0.966 $\pm$ 0.007. This value was used to normalize the fusion-fission event data. The resulting target areal density ratio of ^{236}U to ^{238}U was measured as 1.44 $\pm$ 0.04.

IV. ANALYSIS AND RESULTS

Careful event selection, comprising the majority of the analysis, served as the basis for background reduction and accurate energy measurements.

A. Event selection

The detected particle momentum direction was determined from the struck rings of ΔE and E detectors and was used to exclude events not originating from the target. Due to electronic cross-talk between rings (where neighboring rings would fire sympathetically despite not receiving a true signal), the sector signals were used to determine the energy of the particle. Particles that had enough energy to punch through both the ΔE and E detectors (as determined by the energy loss through the particle telescope), but were not detected by the back L-series detectors, were not included in the analysis because their energy could not be reliably established.

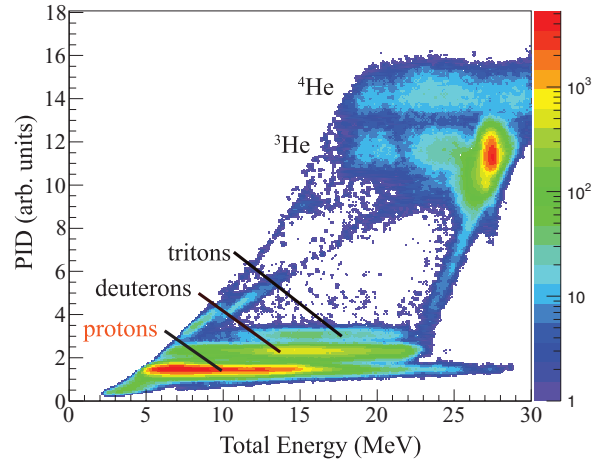

FIG. 3. (Color online) Energy-range plot. Identification of particles (protons, deuterons, tritons, ^{3}He, and ^{4}He) can be made using the PID figure of merit (see text).

The ΔE-E telescope was used to identify particles based on their varying $\frac{dE}{dx}$ profiles. The following particle identification (PID) equation [17] was used to linearize the data in order to simplify event selection:

$$\mathrm{PID} = [(\Delta E + E + L)^{1.7} - (E + L)^{1.7}]\cos\theta, \qquad (7)$$

where ΔE, E, and L are energies measured by the ΔE, E, and L-series back detectors respectively, and θ is the angle between the detector normal and the momentum direction of the projectile, as determined from the struck ΔE and E rings. The resulting energy-range plot is shown in Fig. 3. Protons selected using Eq. (7) were checked for fission coincidence. Only fission events above about 25 MeV (a value that varied with angle due to fission fragment straggle) were accepted, thus excluding light ion events (Fig. 4). A similar rate of light-ion background in the fission detector was seen in the ^{12}C data. Gating on prompt-fission events on the particle-fission timing spectrum (Fig. 5) removed random coincidence events. Random coincidence background was subtracted from the prompt-fission gate by subtracting off-prompt gate random events normalized by the ratio of gate widths. For each event, the proton energy was corrected for losses incurred at detector dead layers and the δ shield degrader foil. The excitation energy of the struck nucleus was then determined from the measured proton energy, the reaction Q value, and the calculated recoil energy of the nucleus. Since the Q values of the two reactions differed by only 5 keV, a value smaller than the detector energy resolution, particle energies translated to the same excitation energies for each reaction.

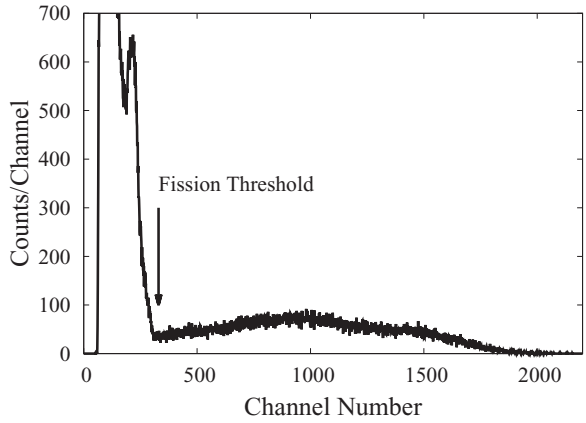

FIG. 4. Typical fission detector energy spectrum (shown here for rings 8–11). The general area of the threshold is marked, though the actual threshold differed slightly for each ring. The threshold is at approximately 25 MeV, to exclude light ions which all have lower energies. Light and heavy fission fragment peaks are discernible around channels 1500 and 1000, respectively.

B. Fission anisotropy

Fission fragments may be emitted in an anisotropic distribution with respect to the reaction plane defined by the scattered particle and the recoiling nucleus [18]. Due to the fission detector's finite solid angle, the differences in the anisotropy between the two targets may influence the fission detector efficiency and impact the accuracy of Eq. (6). An anisotropy can be observed by studying the ratio of the number of in-plane events to out-of-plane events. If the scattered particle was detected in the ΔE sector in line with the fission fragment sector hit, or in the sector 180° opposite, the event was classified as in-plane. A scattered particle detected in a sector 90° offset from the fission event sector classified the event as out-of-plane. The resulting anisotropies for each target are plotted in Fig. 6.

The ratio between the anisotropies for the two targets is consistent with unity over the full range of the investigated neutron energies, indicating that the approximation $\frac{\epsilon_{f2}}{\epsilon_{f1}} \approx 1$ is applicable.

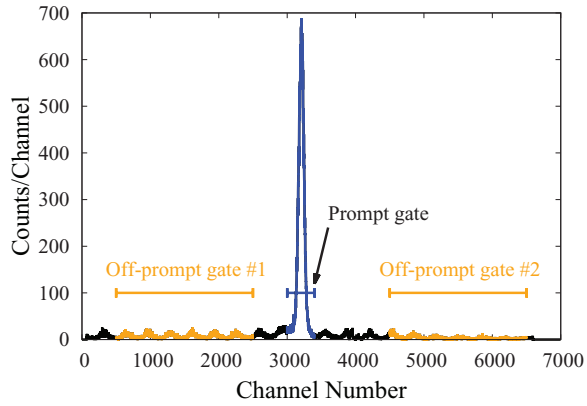

FIG. 5. (Color online) Particle-fission time-to-amplitude spectrum. The prompt fission gate (blue) and off-prompt random gate (orange) are marked. The periodic structure of the accidental particle-fission background is consistent with the cyclotron frequency.

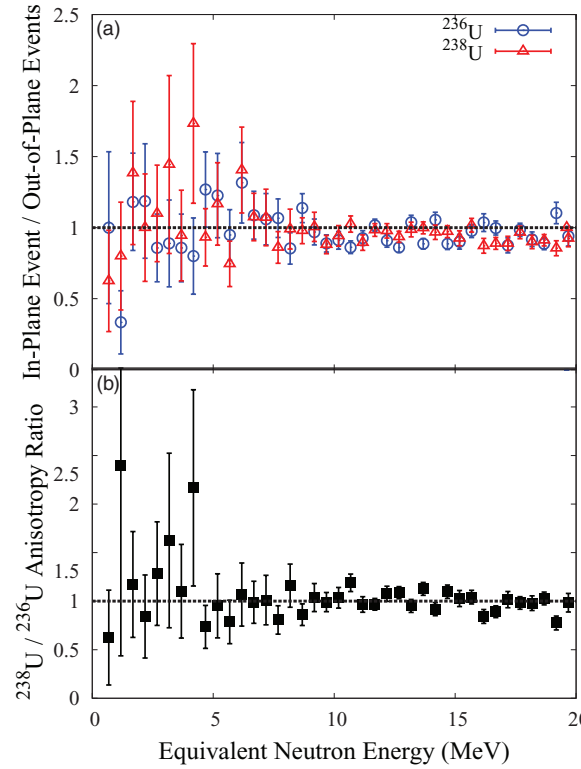

FIG. 6. (Color online) Upper panel: In-plane to out-of-plane fission anisotropy ratios for each target. Values close to unity indicate that the fission fragments were emitted isotropically. Lower panel: Ratio of the fission anisotropies between the two targets. The resulting ratio of anisotropies of the two nuclei is unity within experimental errors.

C. Obtaining the ^{239}Np(n, f) cross section

The proton-fission coincidences for the ^{236}U and ^{238}U targets are shown in Fig. 7. The drop-off in events seen above 16 MeV in excitation energy of the nucleus (corresponding to decreasing proton energy) can in part be attributed to the proton events having lower energy than the height of the Coulomb barrier (at about 15.5 MeV). These lower energy protons are also more likely to get stopped at the ΔE detector, compounding the decrease in events. There is also a drop-off in events at excitation energies below 15 MeV (corresponding to increasing proton energy) that can be attributed to the limited solid angle covered by the L-series detectors needed to stop the higher energy protons. However, both of the reactions are affected in the same way due to identical detector geometry, and hence the ratio of the reactions lacks this dependence.

The normalization factor given in Eq. (5) for the two proton spectra consists of the ratio of target areal thicknesses, live time fractions, and total charge delivered. Total charge was measured by a Faraday cup and integrated over the whole run for each target. Similarly, the live time fraction was measured by comparing the total number of trigger events to the total number of digitized events and was about 95%.

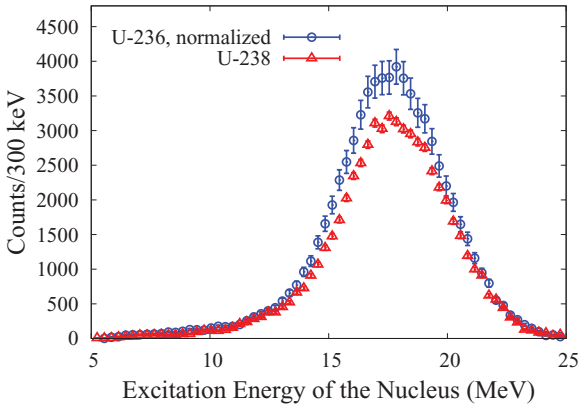

FIG. 7. (Color online) Histograms of background-subtracted proton events coincident with fission for each target as a function of excitation energy of the nucleus. ^{236}U data were normalized to ^{238}U using the target thickness ratio, live time ratio, and total charge delivered.

The normalization factor C was found to be 0.91 ± 0.04. The ratio ^{238}U(^{3}He, pf)/^{236}U(^{3}He, pf), shown in Fig. 8, was obtained by dividing the ^{238}U proton spectrum by the normalized ^{236}U proton spectrum. The reference spectrum of ^{237}Np(n, f) was shifted to excitation energies of the nucleus by adding the neutron separation energy of ^{238}Np, 5.49 MeV. The ratio was then multiplied by the ^{237}Np(n, f)(E_{ex}) cross section [14], resulting in the ^{239}Np(n, f) cross section in excitation energies. The cross section's energy scale was shifted back to neutron-equivalent energies by subtracting the neutron separation energy of ^{240}Np, 5.07 MeV, from the energy scale. Figure 9 shows the cross section.

D. Uncertainties

The statistical uncertainties ranged between 2% and 30% across the energy bins. This was combined in quadrature with the uncertainty in the normalization factor, C, to determine the overall cross-section uncertainty, which ranged between 4% and 30%. An overall energy resolution of ∼120 keV was estimated from energy straggle in the δ shield and the target

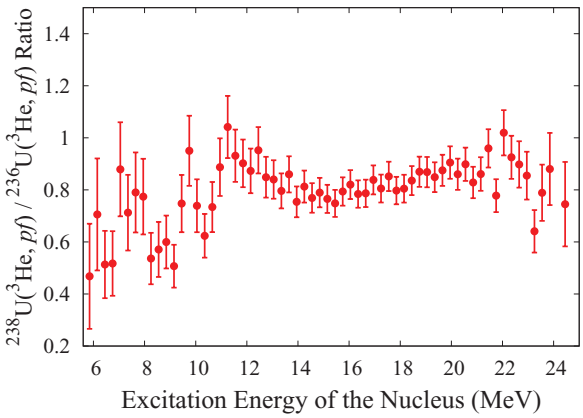

FIG. 8. (Color online) Ratio of ^{238}U(^{3}He, pf) to ^{236}U(^{3}He, pf) events, as a function of the excitation energy of the respective nucleus. The bin size is 300 keV.

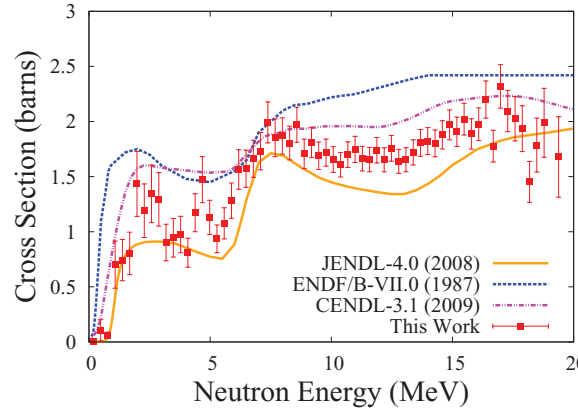

FIG. 9. (Color online) Comparison of the ^{239}Np(n, f) cross section obtained with the SRM to the ENDF/B-VII.0 [19], JENDL-4.0 [20], and CENDL-3.1 [21] evaluations.

(estimated to be 4–27 keV using the ELAST software [22]), intrinsic detector resolution (∼90–100 keV, as determined from the full width at half maximum of calibration spectral peaks), cyclotron beam energy resolution (60 keV, as measured in a previous experiment [5]), and finite angular resolution (causing uncertainty in recoil angle and hence particle energy of about 10–20 keV). The energy uncertainty, determined from the errors of the energy calibration fit parameters, was less than 100 keV, which is well within the chosen 300-keV energy bin widths.

V. DISCUSSION

The cross section, shown in comparison to evaluations in Fig. 9, reveals the expected nuclear structure features, with first and second chance fission evident around 2 and 6 MeV, respectively. The third chance fission is faintly discernible around 15 MeV.

The shape of the cross section parallels most closely the JENDL-4.0 (also the basis for ENDF/B-VII.1) evaluation [20], with the measured cross section being higher by approximately 20% over all the investigated energies. The cross section falls below the CENDL-3.1 and an older ENDF/B-VII.0 (identical to the newest ROSFOND) evaluation. The JENDL-4.0 evaluation uses the ^{238}Np fission barrier parameters to estimate the cross section of ^{239}Np. The 20% discrepancy may indicate that the JENDL-4.0 values are slightly underestimating the fission barrier parameters, although the agreement over the shape validates the CCONE code used in JENDL-4.0 [23].

VI. CONCLUSION

In summary, the first indirect experimental determination of the ^{239}Np(n, f) cross section was performed using the surrogate ratio method. The ^{238}U(^{3}He, pf)^{240}Np reaction was used as a surrogate for the ^{239}Np(n, f)^{240}Np reaction, and the ^{236}U(^{3}He, pf)^{238}Np reaction was used as a surrogate for the directly measured ^{237}Np(n, f)^{238}Np reaction. It was assumed that the direct reaction cross sections, as well as

the compound nucleus formation cross sections for the two surrogate reactions, were nearly equal, since the target nuclei were similar in structure. Using the surrogate ratio method ensured that the effect of contaminants and target backing on the result was minimized, and the uncertainties arising from angular momentum and anisotropy effects were diminished. The total uncertainties were less than 10% over the neutron energy range of 6–18 MeV, giving a relatively good agreement to the JENDL-4.0 evaluation.

The SRM has been successfully benchmarked and employed in the past to measure various neutron-induced fission cross sections, giving confidence to these results. The method could be potentially extended to measure other cross sections needed for nuclear science and technology applications [1], such as neutron-capture reaction cross sections.

ACKNOWLEDGMENTS

We acknowledge Dr. Satoshi Chiba for useful discussions and advice. We also thank the 88-Inch Cyclotron operations and facilities staff for their help with performing the experiment. This work was performed by Lawrence Berkeley National Laboratory and supported by the Director, Office of Energy Research, Office of High Energy and Nuclear Physics, Division of Nuclear Physics, of the US Department of Energy under Contract No. DE-AC02-05CH11231; the US Department of Energy, Lawrence Livermore National Laboratory under Contract No. DE-AC52-07NA27344; the Department of Energy, NNSA, Office of Non-Proliferation (NA-22); the US Department of Homeland Security under Contract No. ARI-022; and NSERC.

[1] G. Aliberti, G. Palmiotti, M. Salvatores, T. Kim, T. Taiwo, M. Anitescu, I. Kodeli, E. Sartori, J. Bosq, and J. Tommasi, Ann. Nucl. Energy **33**, 700 (2006).
[2] J. D. Cramer and H. C. Britt, Nucl. Sci. Eng. **41**, 177 (1970).
[3] J. E. Escher, J. T. Burke, F. S. Dietrich, N. D. Scielzo, I. J. Thompson, and W. Younes, Rev. Mod. Phys. **84**, 353 (2012).
[4] C. Plettner *et al.*, Phys. Rev. C **71**, 051602 (2005).
[5] J. T. Burke *et al.*, Phys. Rev. C **73**, 054604 (2006).
[6] S. R. Lesher *et al.*, Phys. Rev. C **79**, 044609 (2009).
[7] B. L. Goldblum *et al.*, Phys. Rev. C **80**, 044610 (2009).
[8] J. J. Ressler *et al.*, Phys. Rev. C **83**, 054610 (2011).
[9] R. O. Hughes *et al.*, Phys. Rev. C **85**, 024613 (2012).
[10] V. F. Weisskopf and D. H. Ewing, Phys. Rev. **57**, 472 (1940).
[11] W. Hauser and H. Feshbach, Phys. Rev. **87**, 366 (1952).
[12] J. E. Escher and F. S. Dietrich, Phys. Rev. C **74**, 054601 (2006).
[13] S. Chiba and O. Iwamoto, Phys. Rev. C **81**, 044604 (2010).
[14] M. Chadwick *et al.*, Nucl. Data Sheets **112**, 2887 (2011).
[15] S. Lesher, L. Phair, L. Bernstein, D. Bleuel, J. Burke, J. Church, P. Fallon, J. Gibelin, N. Scielzo, and M. Wiedeking, Nucl. Instrum. Methods A **621**, 286 (2010).
[16] M. Herman *et al.*, Nucl. Data Sheets **108**, 2655 (2007).
[17] F. S. Goulding and D. A. Landis, *Recent Advances in Particle Identifiers at Berkeley*, in Semiconductor Nuclear-Particle Detectors and Circuits, Publication 1593 (National Academy of Sciences, Washington, DC, 1969), p. 757.
[18] R. Vanderbosch and J. R. Huizenga, *Nuclear Fission* (Academic, New York, 1973).
[19] M. Chadwick *et al.*, Nucl. Data Sheets **107**, 2931 (2006).
[20] K. Shibata *et al.*, J. Nucl. Sci. Technol. **48**, 1 (2011).
[21] Z. Ge, Z. Zhao, H. Xia, Y. Zhuang, T. Liu, J. Zhang, and H. Wu, J. Korean Phys. Soc. **59**, 1052 (2011).
[22] Adapted from the computer program ENELOSS, written by H. Ernst (1981) with stopping power routines by K. Lesko (1984).
[23] O. Iwamoto, T. Nakagawa, N. Otuka, S. Chiba, K. Okumura, and G. Chiba, J. Nucl. Sci. Technol. **46**, 510 (2008).